*Progress In Electromagnetics Research, PIER 86, 135–154, 2008*

# A TWO-SLOT ARRAY ANTENNA ON A CONCENTRIC SECTORAL CYLINDRICAL CAVITY EXCITED BY A COUPLING SLOT

**P. Wounchoum**

Department of Telecommunication Engineering
Faculty of Engineering
King Mongkut's Institute of Technology Ladkrabang
Bangkok 10520, Thailand

**D. Worasawate**

Department of Electrical Engineering
Faculty of Engineering
Kasetsart University
Bangkok 10900, Thailand

**C. Phongcharoenpanich and M. Krairiksh**

Department of Telecommunication Engineering
Faculty of Engineering
King Mongkut's Institute of Technology Ladkrabang
Bangkok 10520, Thailand

**Abstract**—A two-slot array antenna on a concentric sectoral cylindrical cavity excited by a coupling slot is investigated. The electromagnetic fields and $Q$ factors for the first few modes of a concentric sectoral cylindrical cavity are presented. It shows that the appropriate mode for a slot array antenna on a concentric sectoral cylindrical cavity is the $TM_{110}$ mode. The correlations between each mode distribution and the magnetic field distributions inside the cavity are presented. The antenna design and the parametric study of a two-slot array antenna on a concentric sectoral cylindrical cavity for a single sector are illustrated. Simulated results are validated by measurements. The results provide useful information for the design of a switched-beam slot array antenna on the concentric sectoral cylindrical cavities.

## 1. INTRODUCTION

Slot array antennas have been widely used for many applications due to its conformal nature, compact structure, high power handing, and high efficiency. Many researches on slot antennas have been extensively studied on different structures such as rectangular waveguides [1–7], spheroids [8], infinitely long cylinders [9–11], circular cylindrical cavities [12] and coaxial cables [13–17]. Slot antennas on sectoral cylindrical waveguides have been studied in [18–22]. An impedance characteristic of a sectoral cylindrical cavity-backed slot antenna excited by a probe was presented by [23, 24]. To the best of our knowledge, a concentric sectoral cylindrical cavity-backed slot array antenna excited by a coupling slot has not been analyzed.

This paper focuses on a two-slot array antenna on a concentric sectoral cylindrical cavity excited by a coupling slot. All slots are circumferentially oriented. The antenna is intended for using in a wireless sensor network. A switched-beam antenna, compositing of several antennas covering different sensing areas, is desirable for a master node. The operating frequency of 5.8 GHz ISM band is used for the sensor-size minimization. The goal of this paper is to study the magnetic field distributions inside the slotted cavity and the effects on the antenna characteristics. The magnetic fields for the first few modes inside the cavity with the sectoral angle of 60 degrees are presented. The dimensions of the cross section of the cavity are obtained by considering the solutions for a coaxial cylindrical cavity given in [25, 26] and a circular sectoral waveguide given by [20]. The relations between the outer radius (in terms of wavelength) and the ratio of the inner to outer radii are illustrated. The results show the effects of these parameters on the $TM_{110}$ mode which is easily excited by a coupling slot and provide a uniformly distributed magnetic field on the outer metal wall. $Q$ factors are obtained from the losses of metal wall by using the surface impedance method [25–27]. The $Q$ factor is used to set the optimum dimensions of the cavity. The relations between the ratio of the inner to outer radii and the $Q$ factor are illustrated for $TM_{11q}$ modes. The correlations between each mode distribution and the magnetic field distributions inside the cavity are presented. Computer Simulation Technology (CST) was used as a simulation tool to obtain the antenna characteristics. The radiation pattern, magnetic field distribution and magnitude of $S_{11}$ are investigated in the terms of the length of the cavity. The location of the coupling slot is considered to find the appropriate antenna characteristics. The prototyped antenna was fabricated and measured to verify the simulated results. The results provide useful information

for the design of a switched-beam slot array antenna on the concentric sectoral cylindrical cavities.

## 2. CONCENTRIC SECTORAL CYLINDRICAL CAVITY

### 2.1. Electromagnetic Solutions for a Concentric Sectoral Cylindrical Cavity

The geometry of a concentric sectoral cylindrical cavity is shown in Fig. 1. The inner and outer radii of the cavity are denoted by $r_a$ and $r_b$, respectively. The cavity is enclosed by conducting surfaces at the angles of $\phi = \phi_1$ and $\phi = -\phi_1$. The height of the cavity is denoted by $l_R$ where the bottom and top of the cavity are at $z = 0$ and $z = l_R$, respectively. The cavity is filled with a dielectric medium with the permittivity of $\varepsilon$ and permeability of $\mu$. The electric field, $\mathbf{E}$, and magnetic field, $\mathbf{H}$, in the cavity can be derived from the magnetic vector potential, $\mathbf{A}$, and the electric vector potential, $\mathbf{F}$ as [27]

$$\mathbf{E}(\mathbf{r}) = \frac{1}{j\omega\mu\varepsilon}\nabla \times \nabla \times \mathbf{A}(\mathbf{r}) - \frac{1}{\varepsilon}\nabla \times \mathbf{F}(\mathbf{r}) \tag{1}$$

$$\mathbf{H}(\mathbf{r}) = \frac{1}{j\omega\mu\varepsilon}\nabla \times \nabla \times \mathbf{F}(\mathbf{r}) + \frac{1}{\mu}\nabla \times \mathbf{A}(\mathbf{r}) \tag{2}$$

These electromagnetic fields can be decomposed into two separated modes: TE and TM modes. For TE modes, $\mathbf{A}$ vanishes and only the $z$-component of $\mathbf{F}$ exists. For TM modes, $\mathbf{F}$ vanishes and only the $z$-component of $\mathbf{A}$ exists. The expressions for the fields of a concentric sectoral cylindrical cavity are obtained by modifying the solutions of a coaxial cylindrical cavity and a circular sectoral waveguide.

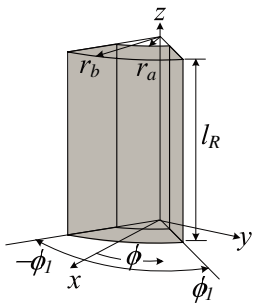


**Figure 1.** Geometry of a concentric sectoral cylindrical cavity.

The expressions for the fields of TE modes are written as

$$\mathbf{F} = A_{pn} B_{\mathrm{TE}}(\rho) \cos(m\phi) \sin(\beta z) \mathbf{a}_z \tag{3}$$

$$E_\rho = A_{pn} \frac{m B_{\mathrm{TE}}(\rho)}{\varepsilon \rho} \sin(m(\phi - \phi_1)) \sin(\beta z) \tag{4}$$

$$E_\phi = A_{pn} \frac{B'_{\mathrm{TE}}(\rho)}{\varepsilon} \cos(m(\phi - \phi_1)) \sin(\beta z) \tag{5}$$

$$E_z = 0 \tag{6}$$

$$H_\rho = A_{pn} \frac{\beta B'_{\mathrm{TE}}(\rho)}{j\omega\mu\varepsilon} \cos(m(\phi - \phi_1)) \cos(\beta z) \tag{7}$$

$$H_\phi = -A_{pn} \frac{m\beta B_{\mathrm{TE}}(\rho)}{j\omega\mu\varepsilon\rho} \sin(m(\phi - \phi_1)) \cos(\beta z) \tag{8}$$

$$H_z = A_{pn} \frac{k_c^2 B_{\mathrm{TE}}(\rho)}{j\omega\mu\varepsilon} \cos(m(\phi - \phi_1)) \sin(\beta z) \tag{9}$$

where subscripts $\rho$, $\phi$, and $z$ denote the radial, circumferential, and axial components of the fields and the $A_{pn}$ values are the amplitudes of the modes associated with subscripts $p = 0, 1, 2, \ldots$, $n = 1, 2, 3, \ldots$ and $m = p\pi/2\phi_1$. The function $B_{\mathrm{TE}}(\rho)$ and its derivative $B'_{\mathrm{TE}}(\rho)$ are defined as

$$B_{\mathrm{TE}}(\rho) = N_m \left( x'_{pn} \frac{\rho}{r_a} \right) - \frac{N'_m(x'_{pn})}{J'_m(x'_{pn})} J_m \left( x'_{pn} \frac{\rho}{r_a} \right) \tag{10}$$

$$B'_{\mathrm{TE}}(\rho) = \frac{x'_{pn}}{r_a} \left[ N'_m \left( x'_{pn} \frac{\rho}{r_a} \right) - \frac{N'_m(x'_{pn})}{J'_m(x'_{pn})} J'_m \left( x'_{pn} \frac{\rho}{r_a} \right) \right] \tag{11}$$

where $x'_{pn}$ is a root of

$$J'_m(x'_{pn}) N'_m(x'_{pn} r_b/r_a) - N'_m(x'_{pn}) J'_m(x'_{pn} r_b/r_a) = 0 \tag{12}$$

and $J_m$, $J'_m$ and $N_m$, $N'_m$ are Bessel functions and their derivatives of order $m$ of the first and second kinds, respectively.

The expressions for the fields of TM modes are written as

$$\mathbf{A} = B_{pn} B_{\mathrm{TM}}(\rho) \sin(m(\phi - \phi_1)) \cos(\beta z) \mathbf{a}_z \tag{13}$$

$$E_\rho = -B_{pn} \frac{\beta B'_{\mathrm{TM}}(\rho)}{j\omega\mu\varepsilon} \sin(m(\phi - \phi_1)) \sin(\beta z) \tag{14}$$

$$E_\phi = -B_{pn} \frac{m\beta B_{\mathrm{TM}}(\rho)}{j\omega\mu\varepsilon\rho} \cos(m(\phi - \phi_1)) \sin(\beta z) \tag{15}$$

$$E_z = B_{pn}\frac{k_c^2 B_{\mathrm{TM}}(\rho)}{j\omega\mu\varepsilon}\sin(m(\phi-\phi_1))\cos(\beta z) \tag{16}$$

$$H_\rho = B_{pn}\frac{mB_{\mathrm{TM}}(\rho)}{\mu\rho}\cos(m(\phi-\phi_1))\cos(\beta z) \tag{17}$$

$$H_\phi = -B_{pn}\frac{B'_{\mathrm{TM}}(\rho)}{\mu}\sin(m(\phi-\phi_1))\cos(\beta z) \tag{18}$$

$$H_z = 0 \tag{19}$$

where the $B_{pn}$ values are the amplitudes of the modes associated with subscripts $p = 1, 2, 3, \ldots$, $n = 1, 2, 3, \ldots$ and $m = p\pi/2\phi_1$. The function $B_{\mathrm{TM}}(\rho)$ and its derivative $B'_{\mathrm{TM}}(\rho)$ are defined as

$$B_{\mathrm{TM}}(\rho) = N_m\left(x_{pn}\frac{\rho}{r_a}\right) - \frac{N_m(x_{pn})}{J_m(x_{pn})}J_m\left(x_{pn}\frac{\rho}{r_a}\right) \tag{20}$$

$$B'_{\mathrm{TM}}(\rho) = \frac{x_{pn}}{r_a}\left[N'_m\left(x_{pn}\frac{\rho}{r_a}\right) - \frac{N_m(x_{pn})}{J_m(x_{pn})}J'_m\left(x_{pn}\frac{\rho}{r_a}\right)\right] \tag{21}$$

where $x_{pn}$ is a root of

$$J_m(x_{pn})N_m(x_{pn}r_b/r_a) - N_m(x_{pn})J_m(x_{pn}r_b/r_a) = 0. \tag{22}$$

The relation between $k$, $k_c$, and $\beta$ is given by $k^2 = k_c^2 + \beta^2$ where $k = \omega\sqrt{\mu\varepsilon} = 2\pi/\lambda$ is a wavenumber in the dielectric-filled medium and

$$\beta = \frac{q\pi}{l_R}, \quad \begin{cases} q = 1, 2, 3 \ldots . & \text{for } \mathrm{TE}^z_{pnq} \text{ modes} \\ q = 0, 1, 2 \ldots . & \text{for } \mathrm{TM}^z_{pnq} \text{ modes} \end{cases} \tag{23}$$

where $k_c = \frac{x'_{pn}}{r_a}$ for $\mathrm{TE}^z_{pn}$ modes and $k_c = \frac{x_{pn}}{r_a}$ for $\mathrm{TM}^z_{pn}$ modes.

Equations (12) and (22) show that the roots $x'_{pn}$ and $x_{pn}$ are functions of the ratio of the inner to outer radii, $r_a/r_b$. To obtain $k_c$ for each mode, the ratio $r_a/r_b$ and one of two radii must be given.

The quality factor or the $Q$ factor is given by

$$Q = \frac{2\pi f_r W}{P_d} \tag{24}$$

where $W$ is the energy stored in the cavity, $P_d$ is the losses of the metal walls, and $f_r$ is the resonant frequency. Their expressions are given as

$$W = \frac{\varepsilon}{2}\int\limits_{Vol} |\mathbf{E}|^2\, dv \tag{25}$$

$$P_d = \frac{R_s}{2} \oint\limits_S |\mathbf{a}_n \times \mathbf{H}|^2 \, ds \tag{26}$$

$$f_r = \frac{1}{2\pi\sqrt{\mu\varepsilon}} \sqrt{(k_c)^2 + \left(\frac{q\pi}{l_R}\right)^2} \tag{27}$$

where $\int\limits_{Vol}$ denotes the volume integration over the cavity, $\oint\limits_S$ denotes the surface integration over the surface of the cavity, $\mathbf{a}_n$ is a unit vector pointing outward from the surface of the cavity, and the surface impedance at the resonant frequency is given by $R_s = \sqrt{\pi f_r \mu/\sigma}$. It can be derived from Eqs. (24)–(26) that the $Q$ factor is inversely proportional to $\sqrt{f_r}$ when the electrical dimensions are fixed. In this paper, copper with the conductivity of $\sigma = 5.84 \times 10^7$ S/m is used as the metal wall and the cavity is filled with free space.

## 2.2. Magnetic Field Distribution inside a Concentric Sectoral Cylindrical Cavity

The magnetic field distributions inside a concentric sectoral cylindrical cavity for individual mode are obtained from Eqs. (7)–(9) and Eqs. (17)–(19) for the TE and TM modes, respectively. The sectoral angle of 60 degrees ($\phi_1$ is equal to 30 degrees) is chosen such each antenna covers one of the six regions which the omnidirectional pattern is equally divided. Fig. 2 shows the geometry of $xy$-plane, $xz$-plane, and $yz$-plane that will be used to refer the magnetic field distribution. The magnetic field distributions inside the cavity for the first few modes are plotted, as shown in Figs. 3–5. It is observed that the $TM_{110}$ mode (dominant mode of TM mode) provides a uniform distribution of magnetic field on the curved metal wall and the magnetic field is aligned in $\phi$ direction. The appropriate mode for a circumferential slot array antenna is the $TM_{110}$ mode. The $TE_{11q}$ modes can be excited

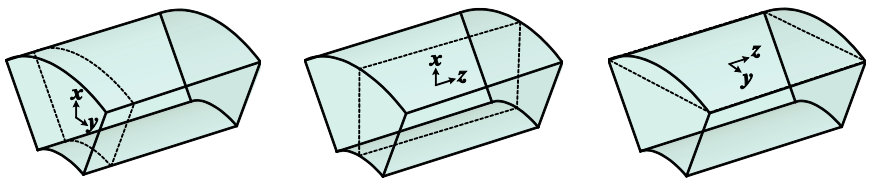


(a) (b) (c)

**Figure 2.** Principal planes for consideration of magnetic field distribution: (a) $xy$-plane, (b) $xz$-plane, (c) $yz$-plane.

when the coupling slot is located at the strong magnetic field position, but do not provide a uniform distribution of magnetic field on the curved metal wall. The $TE_{01q}$ modes cannot be excited by the coupling slot because the magnetic field is aligned in the $z$ direction. Therefore, the distribution of magnetic field of the $TM_{110}$ mode can be easily excited by a coupling slot.

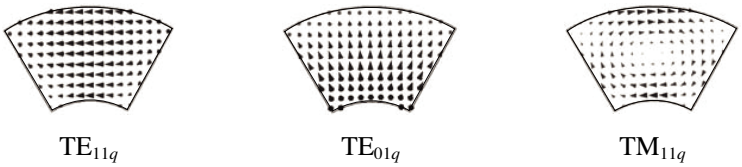


**Figure 3.** Magnetic field inside the cavity in the $xy$-plane.

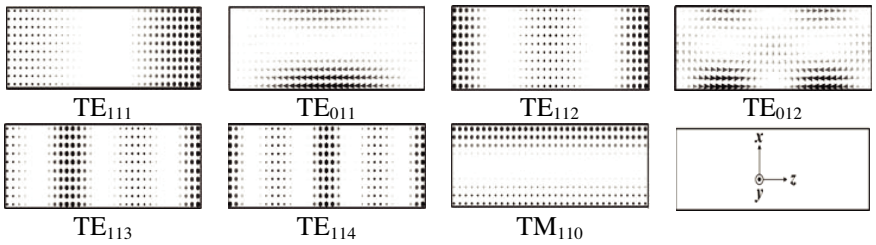


**Figure 4.** Magnetic field inside the cavity in the $xz$-plane.

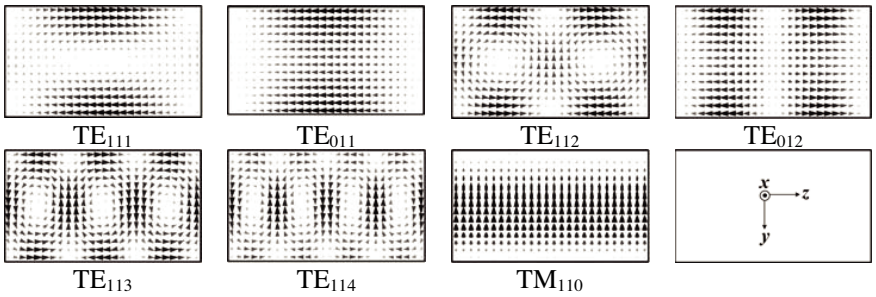


**Figure 5.** Magnetic field inside the cavity in the $yz$-plane.

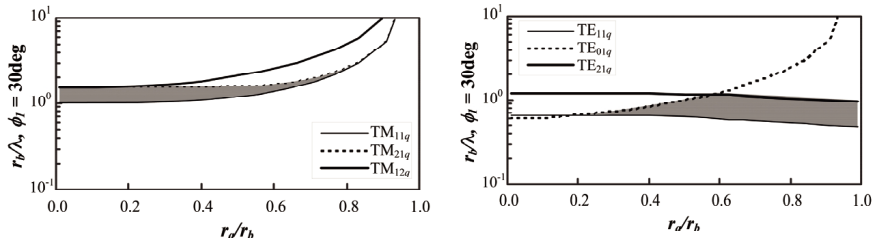


(a) (b)

**Figure 6.** Mode loci for the TE and TM modes: (a) TM, (b) TE.

### 2.3. Effects of Dimensions of the Cross Section on Dominant Modes and Q Factors

This section discusses the effects of the dimensions of the cross section of the cavity on dominant modes using mode loci. The mode locus of each mode is the relation between $r_b/\lambda$ and $r_a/r_b$ for which $k$ is equal to $k_c$ for the specific mode. These relations are obtained from Eqs. (12) and (22). The mode loci for the first few modes are shown in Figs. 6(a) and 6(b) for the TE modes and TM modes. Assuming that only either the TE or the TM modes are excited, the lowest locus indicates the dominant mode. Fig. 6(a) shows the mode loci for the TM modes with $\phi_1 = 30°$. The $TM_{11q}$ mode is a dominant mode for all $r_a/r_b$. However, the width of the valid region for the $TM_{11q}$ mode decreases as $r_a/r_b$ increases. The parameters for which the $TM_{11q}$ mode exists as a single mode are obtained in the shaded region called the valid region. Fig. 6(b) shows the mode loci for the TE modes with $\phi_1 = 30°$. The results show that the dominant mode $TM_{11q}$ is higher mode of the $TE_{11q}$ mode and $TE_{01q}$ mode. The resonant frequency of $TM_{110}$ is the smallest value of $r_b/\lambda$ in the valid region.

The $Q$ factor is used to choose the optimum dimensions of the cavity. Fig. 7 shows the $Q$ factor as a function of $r_a/r_b$ for the $TM_{110}$ mode. The resonant frequency of $TM_{110}$ mode is independent of the height of the cavity. To study the effects of the height of the cavity for $TM_{110}$ mode, the minimum and maximum values of the height of the cavity of $0.5\lambda$ and infinity, respectively, are used. It can be observed that the $Q$ factor of the $TM_{110}$ mode increases as the height of the cavity increases. The maximum $Q$ factor is obtained when the height of the cavity approaches infinity. The $Q$ factor decreases as $r_a/r_b$ increases. The value of $r_a/r_b$ must first be chosen for a high $Q$ cavity then the values of $r_b/\lambda$ is selected from the valid region from the desired height of the cavity.

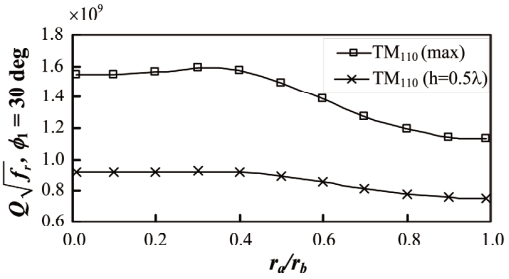


**Figure 7.** $Q\sqrt{f}$ as a function of $r_a/r_b$ for the $TM_{110}$ mode.

### 2.4. Resonances of a Concentric Sectoral Cylindrical Cavity

The inner and outer radii of the concentric sectoral cylindrical cavity are obtained from Section 2.3. The suitable parameters for $TM_{110}$ mode are $r_a/r_b = 0.45$, $r_a = 0.507\lambda$ and $r_b = 1.126\lambda$. The cavity yields a high $Q$ and can be easily excited by the coupling slot from the power divider which is a circular waveguide excited by $TM_{01}$ mode. The resonant length, $l_R$, of the cavity for each mode is shown in Table 1.

**Table 1.** Resonant length of the cavity for each mode.

| Mode | $TE_{111}$ | $TE_{011}$ | $TE_{112}$ | $TE_{012}$ | $TE_{113}$ | $TE_{114}$ | $TM_{110}$ |
|---|---|---|---|---|---|---|---|
| $l_R/\lambda$ | 0.609 | 0.887 | 1.219 | 1.774 | 1.828 | 2.437 | Independent with $l_R$ |

## 3. TWO-SLOT ARRAY ANTENNA ON A CONCENTRIC SECTORAL CYLINDRICAL CAVITY

The antenna structure shown in Fig. 8 consists of two parts, the concentric sectoral cylindrical cavity and the circular waveguide shorted at the top end. It is assumed that the $TM_{01}$ dominant mode propagates in the circular waveguide with the inner radius of $r_c$. The inner and outer radii of the cavity are $r_a$ and $r_b$, respectively. These parameters are considered from the details in Section 2. The coupling slot $S_c$ is on the circular waveguide and centered at ($r = r_a$, $\phi = 0$, $z = l_{sc}$). The radiating slots, $S_1$ and $S_2$ are centered at ($r = r_b$, $\phi = 0$, $z = l_2$) and ($r = r_b$, $\phi = 0$, $z = l_3$), respectively. All slots are circumferentially oriented. The cavity is enclosed by conducting surfaces at the angles of $\phi = -\phi_1$ and $\phi = \phi_1$. The variables $l_1$ and

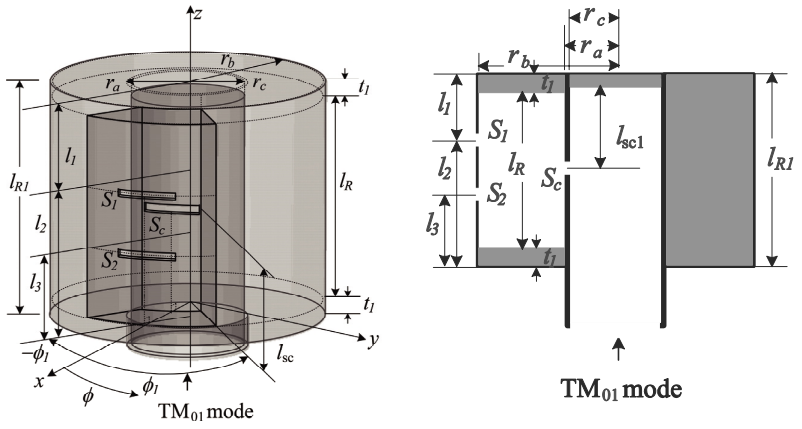


**Figure 8.** Geometry of a two-slot array antenna on a concentric sectoral cylindrical cavity excited by a coupling slot: (a) in 3 dimensions, (b) in 2 dimensions.

$l_3$ are the distance from the top of the cavity to the center of the slot $S_2$ and the distance from the bottom of the cavity to the center of the slot $S_1$. These distances are fixed at $0.75\lambda$. The spacing between the radiating slots is fixed at $0.5\lambda$, for the maximum directivity and the lengths of the radiating slots are fixed at $0.5\lambda$ which is closed to the resonant length given in [22]. The variable $l_{sc1}$, which is the distance from the shorted end of the circular waveguide to the center of the coupling slot, is fixed at $0.5\lambda_g$, where $\lambda_g$ refers to the guided wavelength of the $TM_{01}$ mode of the circular waveguide. The thickness of the top and bottom walls of the cavity is represented by $t_1$. The length of the cavity is $l_R$. Since $l_{R1}$ is fixed, $l_R$ depends on $t_1$. The thickness of the walls $t$ is fixed at 2 mm. The other parameters are also listed in Table 2.

## 4. SIMULATED RESULTS AND DISCUSSION

In this section, the characteristics of the antenna are simulated by using CST Microwave Studio program. The characteristics of the antenna will be investigated as a function of the parameters $l_{sc}$ and $l_R$.

### 4.1. Correlations of Magnetic Field Distributions

In this section, the $FIELD_{\text{ant}}$ is simulated by using CST Microwave Studio program. The values of $FIELD_{\text{ant}}$ are volume quantities of the

**Table 2.** Antenna parameters.

| **Antenna Parameters** | **Electrical Size** | **Physical Size at 5.8 GHz** |
|---|---|---|
| Inner radius of the cavity ($r_a$) | $0.507\lambda$ | 26.20 mm |
| Outer radius of the cavity ($r_b$) | $1.126\lambda$ | 58.23 mm |
| Inner radius of the circular waveguide ($r_c$) | $0.469\lambda$ | 24.20 mm |
| External length of the cavity ($l_{R1}$) | $2.000\lambda$ | 103.44 mm |
| Length of the slot $S_1$ and slot $S_2$ ($L_{S1}$ and $L_{S2}$) | $0.500\lambda$ | 25.86 mm |
| Width of the slot $S_1$ and slot $S_2$ ($W_{S1}$ and $W_{S2}$) | $0.058\lambda$ | 3.00 mm |
| Length of the coupling slot ($L_{SC}$) | $0.480\lambda$ | 24.83 mm |
| Width of the coupling slot ($W_{SC}$) | $0.077\lambda$ | 4.00 mm |

cavity. The spacing between each field observation position is fixed in all directions at 2 mm which are sufficiently accurate to determine the correlations of the magnetic field distributions.

The complex values of $FIELD_{\text{ant}}$ is a phasor representation which can be written in terms of a time-harmonic representation as

$$\tilde{H}_{x,y,z}(t) = |H_{x,y,z}| \cos(\omega t + \angle H_{x,y,z}) \tag{28}$$

where $|H_{x,y,z}|$ and $\angle H_{x,y,z}$ are magnitude and phase of $FIELD_{\text{ant}}$ at the observation position ($x$, $y$, $z$).

The $FIELD_{\text{mode}}$ is the mode distributions of the magnetic field inside the cavity. To find $FIELD_{\text{mode}}$ at a given observation position ($x$, $y$, $z$), the ($x$, $y$, $z$) is scaled and transformed to the cylindrical coordinates and used in (7)–(9) and (17)–(19).

The correlation between $FIELD_{\text{ant}}$ from (28) and $FIELD_{\text{mode}}$, $Corr_{\text{mode}}$, for each mode existing in the antenna is given by

$$Corr_{\text{mode}} = \frac{\langle FIELD_{\text{ant}}, FIELD_{\text{mode}} \rangle}{\sqrt{\langle FIELD_{\text{mode}}, FIELD_{\text{mode}} \rangle}} \tag{29}$$

where $\langle\ \rangle$ is an inner product. Fig. 9 shows an example of the correlation of the magnetic field distributions, as a function of $\omega t$ when $l_R = 0.9\lambda$ and a center-excited coupling slot is used. It is observed that the maximum values of $Corr_{\text{mode}}$ for each mode existing in the antenna occurred at different $\omega t$. From the result, the $Corr_{\text{mode}}$ can

be demonstrated the $FIELD_{\text{mode}}$ of each mode existing in the antenna at each $\omega t$. In addition, the results show that the values of $Corr_{\text{TE111}}$ and $Corr_{\text{TE113}}$ are zero due to the mode cannot be excited.

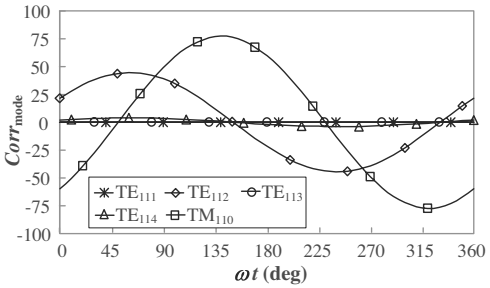


**Figure 9.** Correlations of the magnetic field distributions as a function $\omega t$ with $l_R = 0.9\lambda$.

The total power $P_T$, is the summation of the power for all significant modes defined as

$$P_T = P_{\text{TM110}} + P_{\text{TE111}} + P_{\text{TE112}} + P_{\text{TE113}} + P_{\text{TE114}} \tag{30}$$

and $P_{\text{mode}}(\%)$ is defined as

$$P_{\text{mode}}(\%) = 100 \cdot P_{\text{mode}}/P_T \tag{31}$$

where $P_{\text{mode}} = |Corr_{\text{mode}}|^2_{\text{max}}$. Fig. 10 shows values of $P_{\text{mode}}(\%)$ as a function of $l_R/\lambda$ where the values of $P_{\text{mode}}(\%)$ lower than 0.01% is not plotted. When a center-excited coupling slot (or $l_{sc} = l_R/2$) is used, the values of $P_{\text{mode}}(\%)$ of each mode as a function of $l_R/\lambda$ is shown in Fig. 10(a). It is observed that the maximum and minimum values of $P(\%)_{\text{TM110}}$ occurred at $l_R/\lambda$ equal to 0.60 and 1.22, respectively. In contrast, $l_R/\lambda$ of 0.60 and 1.22 yield the minimum and maximum values of $P_{\text{TE112}}(\%)$, respectively. The values of $P_{\text{TE114}}(\%)$ occurred when the values of $l_R/\lambda$ is greater than 1.6. The values of $P_{\text{TE111}}(\%)$ and $P_{\text{TE113}}(\%)$ are zero due to the mode cannot be excited. When an offset-excited coupling slot (or $l_{sc} = (l_R/2) + 4\,\text{mm}$) is used, a similar trend is observed as shown in Fig. 10(b). However, the values of $P_{\text{mode}}(\%)$ at $l_R/\lambda$ of 0.6–0.9 and 1.6–1.9 have significant effects from the $\text{TE}_{111}$ mode and the $\text{TE}_{113}$ mode, respectively.

### 4.2. Radiation Patterns

Figure 11(a) shows the radiation patterns of the antenna using a center-excited coupling slot. It is obvious that the radiation pattern in $xz$-plane is independent of $l_R$. Due to the excitation by a coupling slot

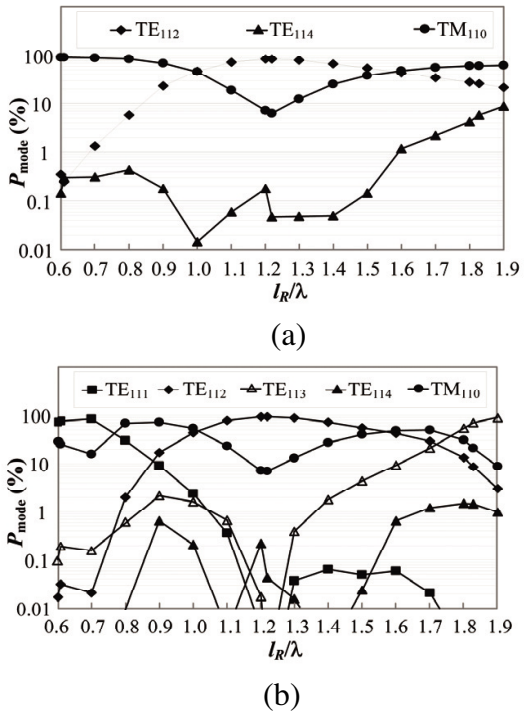


**Figure 10.** Values of $P_{\text{mode}}(\%)$ as a function of $l_R/\lambda$: (a) Center-excited coupling slot, (b) Offset-excited coupling slot.

at the center of $l_R$, the $TE_{111}$ mode and the $TE_{113}$ mode cannot be generated. Therefore, the magnetic fields at both slots are identical.

The radiation patterns of the antenna using an offset-excited coupling slot are shown in Fig. 11(b). The patterns depend on $l_R$ because the $TE_{111}$ mode and the $TE_{113}$ mode can be excited by the coupling slot. The longer values of $l_R/\lambda$ has more effects on the radiation pattern than the shorter values of $l_R/\lambda$, due to the longer values of $l_R/\lambda$ can generate more than one mode. The cavity does not contain a pure component mode of the $TM_{110}$ mode. Therefore, the magnetic fields at both slots are not identical. The radiation patterns in $xz$-plane are tilted downward.

In both cases, the $TE_{011}$ mode and the $TE_{012}$ mode cannot be excited by the coupling slot due to the magnetic field is aligned in the $z$ direction. The $TE_{112}$ mode and the $TE_{114}$ mode can be excited but have no significant effects on the radiation patterns.

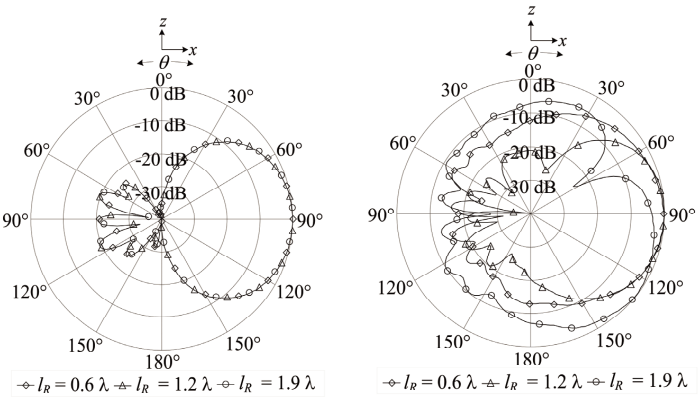


**Figure 11.** Radiation patterns in $xz$-plane (a) Center-excited, (b) Offset-excited.

### 4.3. Directivity and Beam Peak

Figure 12(a) shows the directivity and beam peak in $xz$-plane as a function of $l_R/\lambda$. It is observed that the directivity and the beam peak of the antenna using a center-excited coupling slot are constant at 8.5 dBi and 90 degrees, respectively. When an offset-excited coupling slot is used, the directivity and the beam peak are varied with respect to $l_R$. The directivity decreases almost monotonically as $l_R$. The beam peaks are tilted since the $TE_{111}$ mode and the $TE_{113}$ mode are excited. The maximum beam peaks occur at $l_R/\lambda = 0.7$ and $l_R/\lambda = 1.9$, due to the $TE_{111}$ mode and the $TE_{113}$ mode is fully excited, respectively.

### 4.4. Magnitude of $S_{11}$

Figure 12(b) shows the magnitude of $S_{11}$ as a function of $l_R/\lambda$. When a center-excited coupling slot is used, it is observed that the magnitude of $S_{11}$ increases as $l_R/\lambda$ increases from 0.60–1.22 and the magnitude of $S_{11}$ decreases as $l_R/\lambda$ increases from 1.22–1.80. The maximum magnitude of $S_{11}$ occurs at $l_R/\lambda = 1.22$, due to the $TE_{112}$ mode is fully excited at $l_R/\lambda = 1.22$. The magnitude of $S_{11}$ increases as $l_R/\lambda$ increases from 1.8–1.9, due to the effects of the $TE_{114}$ mode. A similar trend is observed for the antenna using an offset-excited coupling slot. However, the magnitude of $S_{11}$ of the antenna using an offset-excited coupling slot is higher at $l_R/\lambda$ of 0.6–0.7 and 1.7–1.9 due to the $TE_{111}$ mode and the $TE_{113}$ mode are fully excited, respectively.

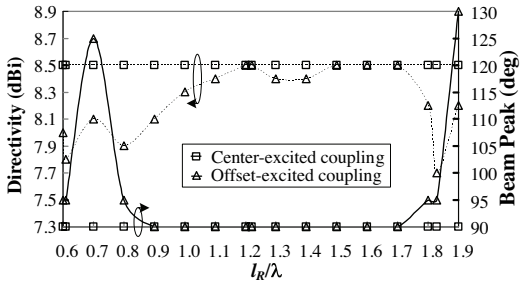


(a)

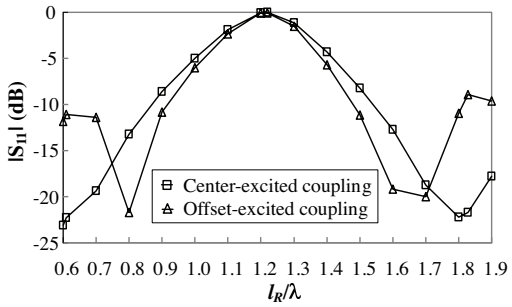


(b)

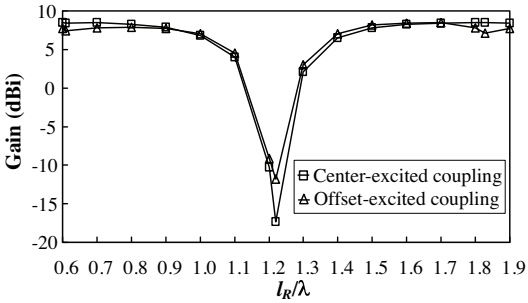


(c)

**Figure 12.** (a) Directivity and beam peak, (b) Magnitude of $S_{11}$, (c) Antenna gain.

A pure component mode of the $TM_{110}$ mode is desired for antenna design. When the center-excited coupling slot is used, the $TE_{111}$ mode and the $TE_{113}$ mode cannot be generated. The $TE_{112}$ mode and the $TE_{114}$ mode can be excited but have no significant effects to the radiation patterns. However, the $TE_{112}$ mode and the $TE_{114}$ mode degraded the magnitude of $S_{11}$ and the maximum magnitude of $S_{11}$

occurred at the mode is fully excited. When the offset-excited coupling slot is used, the $TE_{111}$ mode and the $TE_{113}$ mode can be generated and degrade the radiation patterns due to the magnetic fields at both slots are not identical. In addition, the $TE_{111}$ mode and the $TE_{113}$ mode also degraded the magnitude of $S_{11}$. Figure 12(c) shows the effects on the antenna gain. The existing of other modes degrades the antenna efficiency and causes the antenna gain to decrease.

Therefore, the center-excited coupling slot must be used for optimum antenna characteristics and $l_R$ must be shorter than the resonant length of the cavity for the $TE_{112}$ mode. This will be used as the design guidelines.

## 5. MEASUREMENT RESULTS

To verify the simulated results, the prototyped antenna of the two-slot array antenna on a concentric sectoral cylindrical cavity excited by a coupling slot was fabricated at the operating frequency of 5.8 GHz with the parameters in Table 2 and is shown in Fig. 13. The parameter $l_R/\lambda$ of 0.7 is the suitable design parameter. The monopole on the circular reflector, connected to a SMA connector, is used to excite the $TM_{01}$ mode into the circular waveguide.

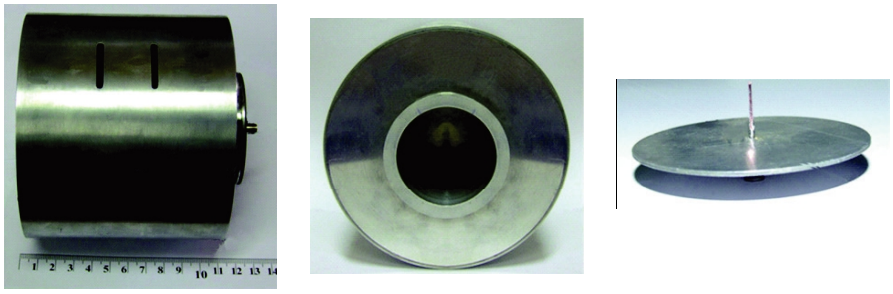

(a) (b) (c)

**Figure 13.** Prototyped antenna: (a) Perspective view, (b) Bottom view, (c) Monopole on the circular reflector.

Figure 14 shows the comparison between the simulated and measured results of the radiation patterns in *xy*- and *xz*-planes. The solid and circle lines are denoted the simulated and measured results, respectively. An excellent agreements are obtained in both in *xy*- and *xz*-planes. Figure 15 shows the measured magnitude of $S_{11}$. The return

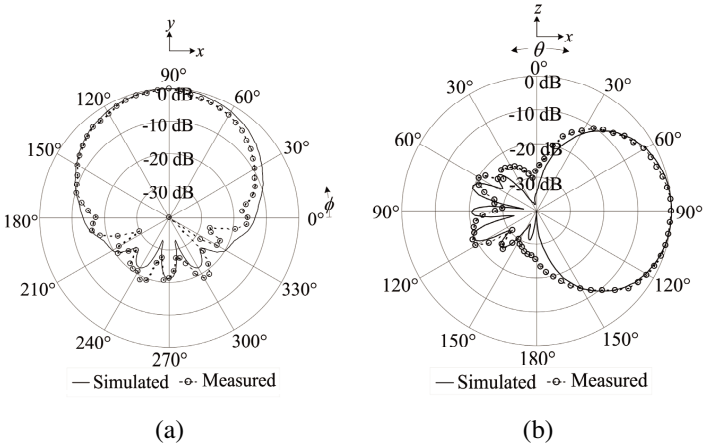


**Figure 14.** Radiation pattern: (a) $xy$-plane, (b) $xz$-plane.

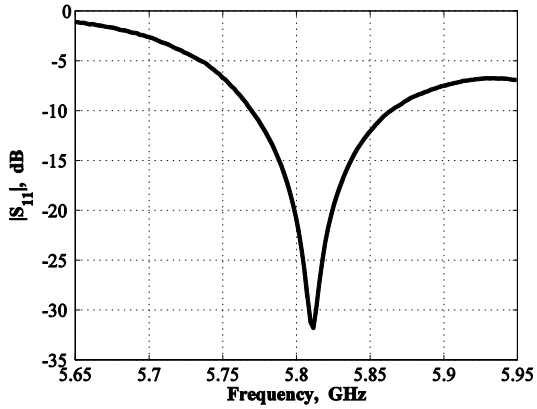


**Figure 15.** Magnitude of $S_{11}$ of the prototyped antenna.

loss of 20.6 dB is obtained at 5.8 GHz. The measured gain at 5.8 GHz is 7.8 dBi.

## 6. CONCLUSION

In this paper, a two-slot array antenna on a concentric sectoral cylindrical cavity excited by a coupling slot is investigated. The electromagnetic solutions and $Q$ factors of a concentric sectoral cylindrical cavity are presented. The relations between the outer

radius and the ratio of the inner to outer radii are studied. The $Q$ factor is used to determine the optimum dimensions of the cavity. The results show that the appropriate mode for a slot array antenna on a concentric sectoral cylindrical cavity is the $TM_{110}$ mode. The correlations between each mode distribution and the magnetic field distributions inside the cavity are presented. The radiation pattern, magnetic field distribution and magnitude of $S_{11}$ are investigated in the terms of the length of the cavity. The results show that when a center-excited coupling slot is used, the $TE_{112}$ mode and $TE_{114}$ mode degraded the magnitude of $S_{11}$.To obtain the high efficiency of the antenna, the suitable parameters are the center-excited coupling slot and the length of the cavity must be shorter than the resonant length of the cavity for the $TE_{112}$ mode. The prototyped antenna was fabricated and measured to verify the simulated results. The results provide useful information for the design of a switched-beam slot array antenna on the concentric sectoral cylindrical cavities.

## ACKNOWLEDGMENT

This work was supported by the Thailand Research Fund (TRF) under the grant number RTA 5180002.

## REFERENCES

1. Liu, H. X., H. Q. Zhai, L. Li, and C. H. Liang, "A progressive numerical method combined with MOM for a fast analysis of large waveguide slot antenna array," *Journal of Electromagnetic Waves and Applications*, Vol. 20, No. 2, 183–192, 2006.
2. Pazoki, R. and J. Rashed-Mohassel, "Bandwidth enhancement of resonant slot array antennas," *Journal of Electromagnetic Waves and Applications*, Vol. 21, No. 9, 1177–1189, 2007.
3. Lim, K. S., V. C. Koo, and T.-S. Lim, "Design, simulation and measurement of a post slot waveguide antenna," *Journal of Electromagnetic Waves and Applications*, Vol. 21, No. 12, 1589–1603, 2007.
4. Mondal, M. and A. Chakrabarty, "Resonant length calculation and radiation pattern synthesis of longitudinal slot antenna in rectangular waveguide," *Progress In Electromagnetics Research Letters*, Vol. 3, 187–195, 2008.
5. Li, L., C.-H. Liang, and C.-H. Chan, "Waveguide end-slot phased array antenna integrated with electromagnetic bandgap

structures," *Journal of Electromagnetic Waves and Applications*, Vol. 21, No. 2, 161–174, 2007.

6. Zhao, X. W., X. J. Dang, Y. Zhang, and C. H. Liang, "MLFMA analysis of waveguide arrays with narrow-wall slots," *Journal of Electromagnetic Waves and Applications*, Vol. 21, No. 8, 1063–1078, 2007.
7. Tiwari, A. K., D. R. Poddar, and B. N. Das, "On the equivalent radius of a radiating slot in impedance calculations," *Progress In Electromagnetics Research*, PIER 74, 47–56, 2007.
8. Hamid, A.-K. and F. R. Cooray, "Radiation characteristics of a spheroidal slot antenna coated with isorefractive materials," *Journal of Electromagnetic Waves and Applications*, Vol. 21, No. 12, 1605–1619, 2007.
9. Shin, D. H. and H. J. Eom, "Radiation from narrow circumferential slots on a conducting circular cylinder," *IEEE Trans. Antennas Propagat.*, Vol. 53, No. 6, 2081–2088, June 2005.
10. Ock, J. S. and H. J. Eom, "Radiation of a hertzian dipole in a short-ended conducting circular cylinder with narrow circumferential slots," *Progress In Electromagnetics Research Letters*, Vol. 2, 11–20, 2008.
11. Hamid, A. K., "Multi-dielectric loaded axially slotted antenna on circular or elliptic cylinder," *Journal of Electromagnetic Waves and Applications*, Vol. 20, No. 9, 1259–1271, 2006.
12. Kim, J. H. and H. J. Eom, "Radiation from multiple annular slots on a circular cylindrical cavity," *Journal of Electromagnetic Waves and Applications*, Vol. 21, No. 1, 47–56, 2007.
13. Wang, J. H. and K. K. Mei, "Theory and analysis of leaky coaxial cables with periodic slots," *IEEE Trans. Antennas Propagat.*, Vol. 49, No. 12, 1723–1732, Dec. 2001.
14. Kim, D. H. and H. J. Eom, "Mode-matching analysis of axially slotted coaxial cable," *IEEE Antennas Wireless Propag. Lett.*, Vol. 4, 169–171, 2005.
15. Ahn, C. H., D. W. Yi, and W. S. Park, "Design of a radiated-mode multislot leaky coaxial cable," *Microw. Opt. Tech. Lett.*, Vol. 45, No. 4, 338–342, May. 2005.
16. Park, J. K., D. H. Shin, J. N. Lee, and H. J. Eom, "A full-wave analysis of a coaxial waveguide slot bridge using the Fourier transform technique," *Journal of Electromagnetic Waves and Applications*, Vol. 20, No. 2, 143–158, 2006.
17. Shin, D. H. and H. J. Eom, "Radiation of a leaky coaxial cable with narrow transverse slots," *IEEE Trans. Antennas Propagat.*,

Vol. 55, No. 1, 107–110, Jan. 2007.

18. Fan, G. X. and J. M. Jin, "Scattering from a cylindrically conformal slotted waveguide array antenna," *IEEE Trans. Antennas. and Propagat.*, Vol. 45, 1150–1159, July 1997.
19. Lin, F. and A. S. Omar, "Segment-sector waveguides," *Proc. 1989 IEEE AP-S Int. Symp.*, 965–968, June 1989.
20. Elsherbeni, A., D. Kajfez, and S. Zeng, "Circular sectoral waveguides," *IEEE Antennas and Propagation Magazine*, Vol. 33, 20–27, Dec. 1991.
21. Lue, S. W., S. C. Li, and S. M. Cao, "Slot antenna in the cuved broad wall of a sectoral waveguide," *Asia-Pacific Microwave Conference 1992*, 401–403, Adelaide, Australia, 1992.
22. Lue, S. W., Y. Zhuang, and S. M. Cao, "The equivalent parameters for the radiating slot on a sectoral waveguide," *IEEE Trans. Antennas Propagat.*, Vol. 42, 1577–1581, Nov. 1994.
23. Wongsan, R., C. Phongcharoenpanich, M. Krairiksh, and J. Takada, "Impedance characteristic analysis of an axial slot antenna on a sectoral cylindrical cavity excited by a probe using Method of Moments," *IEICE Trans. Fundamentals*, Vol. E-86A, 1364–1373, June 2003.
24. Pasri, N., C. Phongcharoenpanich, and M. Krairiksh, "Design of a circumferential slot antenna on a sectoral cylindrical cavity excited by a probe," *Proc. 2004 IEEE AP-S Int. Symp.*, 2337–2340, June 2004.
25. Balanis, C. A., *Advance Engineering Electromagnetics*, John Wiley & Sons, New York, 1989.
26. Miner, G. F., *Lines and Electromagnetic Fields for Engineers*, Oxford University Press, New York, 1996.
27. Harrington, R. F., *Time-Harmonic Electromagnetic Fields*, McGraw-Hill, New York, 1985.